Supplemental Materials for "A model for adult organ resizing demonstrates stem cell scaling through a tunable commitment rate"

XinXin Du, Lucy Erin O'Brien, Ingmar Riedel-Kruse

May 12, 2017

1 Morphological region of Drosophila midgut known to exhibit scaling

The Drosophila midgut consists of five morphologically distinct subregions [1], named R1, R2, R3, R4, and R5. The region that has been shown to exhibit stem cell scaling is the fourth region from the anterior end of the midgut, the R4 region [2] (Figure S1). All cell number data and stem cell scaling phenomena refer to investigation of this region.

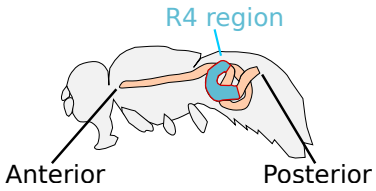

Figure S1: Region of Drosophila midgut (region R4) that is known to exhibit stem cell scaling (blue).

2 Non-spatial model

2.1 Steady state solutions to model equations with constant commitment rate

For the non-spatial model, the model equations are:

$$\begin{aligned}\dot{s} &= a_m \frac{E_d^2}{1+E_d^2} s - bs \\ \dot{u} &= bs - \lambda u \\ \dot{U} &= \lambda u - \Lambda_m \frac{1}{1+E_d^2} U \quad .\end{aligned} \tag{1}$$

where E_d is effective food density. Here E_d is the non-dimensionalization of $E_d^{\dim}$:

$$\begin{aligned}E_d^{\dim} &= \frac{E_{\text{in}}}{A_1 s + A_2 u + A_3 U} \equiv \frac{E_{\text{in}}}{A} \\ E_d &= \frac{E_d^{\dim}}{E_d^0} = \frac{E'_{\text{in}}}{A'_1 s + A'_2 u + A'_3 U} \quad ,\end{aligned} \tag{2}$$

where the quantity E_{in} is the parameter indicating food input. We have $A \equiv A_1 s + A_2 u + A_3 U$ as the total tissue consumption of E_{in}, where A_1, A_2, and A_3 denote the cell-type specific consumption per cell for cell types s, u, and U. The primed parameters E'_{in}, A'_1, A'_2, and A'_3 are dimensionless. In the main text, primes have been dropped for notational convenience. Here E_d^0 denotes a convenient switch point of division rate a as a function of $E_d^{\dim}$ such that:

$$\begin{aligned}a &= a_m \frac{E_d^{\dim 2}}{E_d^{02} + E_d^{\dim 2}} \\ &= a_m \frac{E_d^2}{1+E_d^2} \quad .\end{aligned} \tag{3}$$

Solving Equation 1 under steady state conditions, we have, for the steady state cell number ratios s_0/u_0 and s_0/U_0:

$$s_0/u_0 = \frac{\lambda}{b} \tag{4}$$

$$s_0/U_0 = \Lambda_m \left(\frac{1}{b} - \frac{1}{a_m} \right) \quad , \tag{5}$$

and for s_0,

$$s_0 = \sqrt{\frac{a_m - b}{b}}\, E_{\text{in}} \Bigg/ \left(A_1 + A_2 \frac{b}{\lambda} + A_3 \frac{1}{\Lambda_m} \frac{1}{\left(\frac{1}{b} - \frac{1}{a_m} \right)} \right) \quad . \tag{6}$$

Equations 4, 5, and 6 fully indicate the steady states of the model. Note that if division rate a were $a = a_m E_d^n/(1 + E_d^n)$ and cell death rate Λ were $\Lambda = \Lambda_m/(1 + E_d^n)$ then Equation 6 would be replaced by

$$s_0 = \left(\frac{a_m - b}{b}\right)^{1/n} E_{\text{in}} \Bigg/ \left(A_1 + A_2\frac{b}{\lambda} + A_3\frac{1}{\Lambda_m}\frac{1}{\left(\frac{1}{b} - \frac{1}{a_m}\right)}\right) \quad , \tag{7}$$

while Equations 4 and 5 would be unchanged.

The steady state total tissue consumption is given by:

$$A_1 s_0 + A_2 u_0 + A_3 U_0 = \sqrt{\frac{a_m}{b} - 1}\, E_{\text{in}} \quad . \tag{8}$$

If division rate a were $a = a_m E_d^n/(1 + E_d^n)$ and cell death rate Λ were $\Lambda = \Lambda_m/(1 + E_d^n)$, then the steady state would have:

$$A_1 s_0 + A_2 u_0 + A_3 U_0 = \left(\frac{a_m}{b} - 1\right)^{1/n} E_{\text{in}} \quad . \tag{9}$$

2.1.1 Constant number of stem cells

Here, as an example, we consider the case where tissue size can depend on food, but the number of stem cells is static. This implies putting $b = a$ or $\dot{s} = 0$ in Equation 1 while a still has the dependence on E_d as in Equation 3. We additionally use the definition of frequency of symmetric-stem fate outcomes as in the main text:

$$P(\text{sym}) = \left(\frac{a}{a+b}\right)^2 \quad , \tag{10}$$

to examine this case.

Using the empirical result that total midgut cell number increases by four-fold during growth [2], a value of 4x increase in food was chosen to examine growth and shrinkage in this case. Solving Equation 1 for 4x changes in food, we illustrate that when stem cell numbers are constant, enterocyte numbers U can increase or decrease according to food if Equation 3 is satisfied; this is similar to midgut growth *in vivo* (Figure S2A). However, two other key *in vivo* features cannot be replicated; symmetric-stem fates do not increase, and stem cell scaling does not occur (Figure S2B,C). This is in contrast to a model where s has non-trivial dynamics (Figure S2D-F).

2.2 Range estimation for maximum probability symmetric-stem fate outcomes

The data in [2] Table S4 stated that 72 out of 106 marked divisions (or 68% of marked divisions) were observed to have stem-stem (or "symmetric-stem") fate

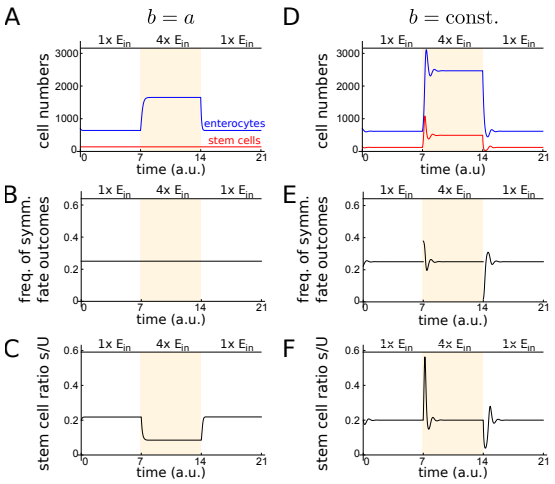

Figure S2: Model (Equation 1) with constant stem cell number ($b = a$, $\dot{s} = 0$) is not compatible with stem cell scaling, while model with $b = \text{const.}$ is compatible. (A-F) Feed-fast cycles in which E_{in} changes at $t = 7$ and $t = 14$ (a.u.) for Equation 1 with constant stem cell number ($b = a$) (A-C) and with $b = \text{const.}$ (D-F). (A,D) Stem cell (red) and enterocyte (blue) numbers as functions of time. (B,E) The frequency of symmetric fate outcomes is transiently increased by increased nutrient density in (E) but not in (B). (C,F) The ratio of stem cells to enterocytes returns to same value after alteration of E_{in} in (F) but not in (C). Hence, constant commitment rate (F) is compatible with stem cell scaling, while commitment rate tuned to division rate (C) is not compatible.

outcomes. If we assume there is *no* biological variability, and that all margin of error of that measurement is due to the limited sample size, then the standard margin of error would be approximately $\sigma = \sqrt{106 * (1 - 0.68) * 0.68)} \approx 4.8$, where we assumed a binomial distribution for symmetric-stem fate outcomes with sample size $N = 106$ and probability of success $p = 0.68$. If we include a range of 2σ on either side of the recorded 72 symmetric-stem fate outcomes, this gives an estimate of 72 ± 10 symmetric-stem fates out of 106 divisions, which gives a range for $P_{\text{max}}(\text{sym})$ of $58\% \leq P_{\text{max}}(\text{sym}) \leq 77\%$ to include a large majority of cases.

Since this calculation is based on the assumption that there is *no* underlying biological variability, the true range of $P_{\text{max}}(\text{sym})$ is likely larger due to biological variability. We currently do not have an estimate of biological variability for $P_{\text{max}}(\text{sym})$. However, given this calculation of the sampling error, we estimate that estimating $P_{\text{max}}(\text{sym})$ within a rough range of 50% to 90% to account for both biological variability and sampling error is appropriate.

2.3 Steady state solutions to model equations for stem cell ratio-dependent commitment rate

In the case where commitment rate b depends on cell densities, we would have b in Equation 1 replaced by $b = B_0 s/U$. The model equations are:

$$\begin{aligned} \dot{s} &= a_m \frac{E_d^2}{1+E_d^2} s - B_0 \frac{s}{U} s \\ \dot{u} &= B_0 \frac{s}{U} s - \lambda u \\ \dot{U} &= \lambda u - \Lambda_m \frac{1}{1+E_d^2} U \quad . \end{aligned} \tag{11}$$

To obtain the steady states $\dot{s} = \dot{u} = \dot{U} = 0$, we set the left hand side of Equation 11 to 0. Algebraic rearrangement will then lead to Equations 4-6 with b replaced by $B_0\, s_0/U_0$. Specifically:

$$s_0/u_0 = \frac{\lambda}{B_0 s_0/U_0} \tag{12}$$

$$s_0/U_0 = \Lambda_m \left(\frac{1}{B_0 s_0/U_0} - \frac{1}{a_m} \right) \tag{13}$$

$$s_0 = \sqrt{\frac{a_m - B_0 s_0/U_0}{B_0 s_0/U_0}}\, E_{\text{in}} \Bigg/ \left(A_1 + A_2 \frac{B_0 s_0/U_0}{\lambda} + A_3 \frac{1}{\Lambda_m} \frac{1}{\left(\frac{1}{B_0 s_0/U_0} - \frac{1}{a_m} \right)} \right) \quad . \tag{14}$$

Noting that Equation 13 is a quadratic equation for s_0/U_0:

$$B_0 \left(\frac{s_0}{U_0} \right)^2 + \frac{\Lambda_m}{a_m} B_0 \frac{s_0}{U_0} - \Lambda_m = 0 \quad , \tag{15}$$

solving, and choosing the positive root, we have:

$$s_0/U_0 = \frac{-\Lambda_m}{2a_m} + \sqrt{\left(\frac{\Lambda_m}{2a_m} \right)^2 + \frac{\Lambda_m}{B_0}} \quad . \tag{16}$$

Substituting the expression for s_0/U_0 from Equation 16 into Equation 12 and 14 gives the steady states of s_0/u_0 and stem cell number s_0 in terms of input parameters. Equations 16, 12, and 14 give the full steady state solutions to Equation 11.

2.4 Linear stability analysis of steady states for constant commitment rate model ($b = \text{const.} \equiv B_0$)

Denoting $\dot{s} \equiv f(s,u,U)$, $\dot{u} \equiv g(s,u,U)$, and $\dot{U} \equiv h(s,u,U)$ in Equation 1, we evaluate the Jacobian at the steady state of the constant commitment rate

model (Equation 1) to obtain:

$$J_0 = \begin{pmatrix} \frac{\partial f}{\partial s} & \frac{\partial f}{\partial u} & \frac{\partial f}{\partial U} \\ \frac{\partial g}{\partial s} & \frac{\partial g}{\partial u} & \frac{\partial g}{\partial U} \\ \frac{\partial h}{\partial s} & \frac{\partial h}{\partial u} & \frac{\partial h}{\partial U} \end{pmatrix} \Bigg|_{s=s_0,\, u=u_0,\, U=U_0} = \begin{pmatrix} -\frac{A_1 P}{Q} & -\frac{A_2 P}{Q} & -\frac{A_3 P}{Q} \\ b & -\lambda & 0 \\ -\frac{A_1 P b}{Q} & \frac{P_1}{Q} & -\frac{P_2}{Q} \end{pmatrix} \tag{17}$$

where P, P_1, P_2, and Q are introduced for notational convenience:

$$P = 2b\lambda\Lambda_m(a_m - b)^2 \tag{18}$$

$$P_1 = \lambda^2 a_m^2 b A_3 + \lambda\Lambda_m(a_m - b)\left(bA_2(a_m - 2b) + a_m\lambda A_1\right) \tag{19}$$

$$P_2 = \Lambda_m(a_m - b)\left(b\lambda A_3(a_m + 2b) + \Lambda_m(a_m - b)(A_2 b + A_1\lambda)\right) \tag{20}$$

$$Q = a_m^2 b\lambda A_3 + a_m\Lambda_m(a_m - b)(A_2 b + A_1\lambda) \quad . \tag{21}$$

Due to the fact that the steady states of Equation 1 scale with the input E_{in}, we have that J_0 does not depend on E_{in}.

We numerically evaluated the eigenvalues of J_0 for the same range of parameter values as Figure 2A,B of the main text. Our analysis shows that for many parameter values, steady state solutions to Equation 1 have oscillations about the steady state; that is, eigenvalues of J_0 contain complex conjugates (black, gray, or white markers in Figure S3A). Moreover, for many parameter values (black diamonds in Figure S3A) we find that solutions to Equation 1 have "large" oscillations about the steady state. Here, we characterize "large" oscillations about the steady state by the property that $|\operatorname{Im}(e_1)|/|\operatorname{Re}(e_1)| > 5$, where e_1 is an eigenvalue of J_0 whose complex conjugate also an eigenvalue of J_0. The ratio $|\operatorname{Im}(e_1)|/|\operatorname{Re}(e_1)|$ can be roughly interpreted as the number of oscillations in the solution before it closely approximates homeostasis. From qualitative examination, solutions with $|\operatorname{Im}(e_1)|/|\operatorname{Re}(e_1)| > 5$ had oscillations that seemed extensive, while solutions with $|\operatorname{Im}(e_1)|/|\operatorname{Re}(e_1)| < 1$ seemed close to non-oscillatory. In Figure S3, the terms "small", "medium", and "large" oscillations are used to indicate values of $|\operatorname{Im}(e_1)|/|\operatorname{Re}(e_1)|$ that fall in different numerical ranges of $|\operatorname{Im}(e_1)|/|\operatorname{Re}(e_1)| < 1$, $1 \leq |\operatorname{Im}(e_1)|/|\operatorname{Re}(e_1)| < 5$, and $|\operatorname{Im}(e_1)|/|\operatorname{Re}(e_1)| < 5$, respectively.

Additionally, denoting the eigenvalues of J_0 as e_1, e_2, and e_3, we evaluate the rate of approach ν to the steady state from the slowest eigendirection, i.e. $\nu \equiv \min\{|\operatorname{Re}(e_1)|, |\operatorname{Re}(e_2)|, |\operatorname{Re}(e_3)|\}$. Assuming that the time to homeostasis for the midgut is 3.5 days [2], we have that the rate of approach ν to the steady state that would allow the system to be within 10% of homeostasis in 3.5 days should satisfy:

$$\text{time to within 10\% of homeostasis} = \frac{3.5}{\ln 0.1} > \frac{1}{\nu} \quad . \tag{22}$$

Parameters with ν satisfying Equation 22 (green markers in Figure figsupp:lin) roughly correspond to the white areas in Figure 3A of the main text, see Figure S3C.

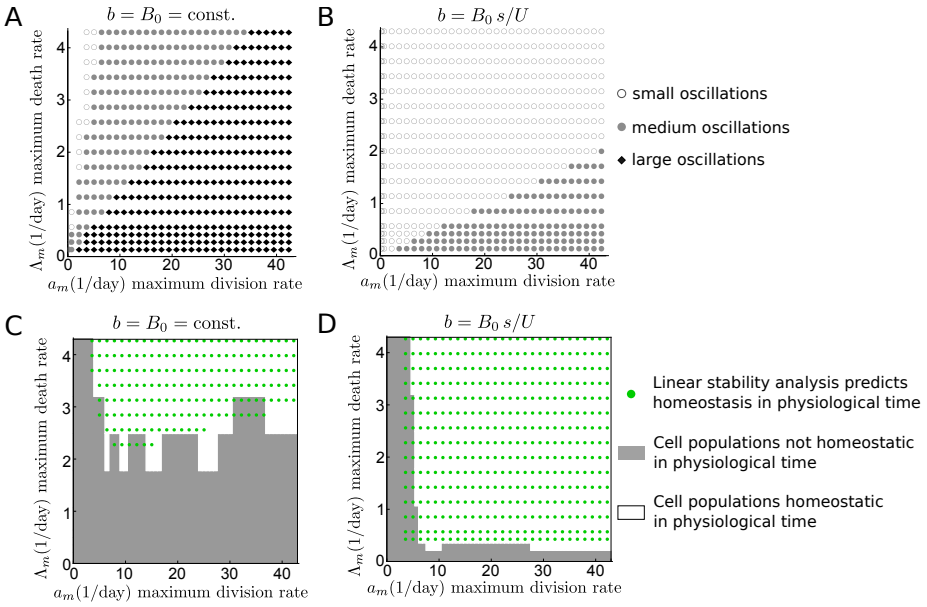

Figure S3: Linear stability analysis of the steady states of Equations 1 and 11 shows that incorporating stem cell proportion-dependent commitment rate reduces oscillations (A,B) and increases rate of approach to the steady state (C,D). (A,B) Plot markers indicate parameter values for which there are oscillations about the steady state for the $b = B_0$ model (A) and the $b = B_0\, s/U$ model (B). For e_1 an eigenvalue of J_0 (A) or J_0' (B) whose complex conjugate also an eigenvalue, open gray circles have $0 < |\operatorname{Im}(e_1)|/|\operatorname{Re}(e_1)| < 1$, solid gray circles have $1 \leq |\operatorname{Im}(e_1)|/|\operatorname{Re}(e_1)| < 5$, and black diamonds have $\operatorname{Im}(e_1)|/|\operatorname{Re}(e_1)| > 5$. (C,D) Green points indicate parameter values for which the slowest rate of approach ν to the steady state is consistent with solutions reaching homeostasis within $t = 3.5$ days, indicated for Equation 1 (C) and 11 (D). Numerical characterization of whether system reaches approximate homeostasis in physiological time are shown in gray and white.

2.5 Linear stability analysis of steady states for stem cell proportion-dependent commitment rate model ($b = B_0 s/U$)

We denote by J_0' the Jacobian of the stem cell proportion-dependent commitment rate model (Equation 11), evaluated at the steady state indicated in Equations 12, 14, and 16. Note again that J_0' does not depend in E_{in}. We similarly examine the eigenvalues of J_0' for the parameter values in Figure 3A,B of the main text. We find that in this parameter space, there are no solutions to this model that have "large" oscillations about the steady state (i.e. no black diamond markers exist in Figure S3B). In fact, in this parameter space, all eigenvalues e_1 of J_0' whose complex conjugate is also an eigenvalue of J_0', satisfy $|\operatorname{Im}(e_1)|/|\operatorname{Re}(e_1)| < 1.4$.

Additionally, we characterized the rate of approach ν to the steady state from the slowest eigendirection and find again that parameters with ν satisfying Equation 22 (green markers in Figure figsupp:lin) roughly correspond to the white areas in Figure 3B of the main text, see Figure S3D.

2.6 Conditions to determine whether Equation 1 has reached approximate steady state

We define conditions under which solutions $s(t)$, $u(t)$, and $U(t)$ to the system in Equation 1 can be considered to have reached "approximate steady state" or "approximate homeostasis" at time T for Figure 2 of the main text. We use the enterocyte population U in these conditions since intestinal enterocytes in the midgut contribute the most to the midgut's functionality as a digestive organ. Our first condition for approximate equilibrium is $|U(T) - U_0|/U_0 < 0.05$ where U_0 is the steady state value of enterocyte. This condition requires that values of enterocytes should be close to U_0 for the system to be close to homeostasis. Our second condition is that the derivative U' should satisfy $|U'(T)| < 0.15 * \sup_t |U'(t)|$, requiring that the function $U(t)$ should not be changing rapidly at $t = T$. Our results are not sensitive to the specifics of these conditions.

2.7 Incompatible dynamics of $b = B_0$ model with experimental measurements for a variety of model details

To show that a constant commitment rate model gives rise to poor compatibility of Equation 1 with experimental measurements and that feedback in the commitment rate b strongly improves the compatibility, we varied model details and solved Equation 1 with $b = B_0$ and $b = B_0 s/U$ to compare their parameter spaces.

We show that the non-spatial model with constant commitment rate $b = B_0$ remains incompatible with experimental measurements for a range of model details. In contrast, the non-spatial model with feedback in the commitment rate $b = B_0 s/U$ remains compatible with experimental measurements for similar ranges of experimental details. Moreover, for the same set of model details and parameter regimes, the non-spatial model with $b = B_0 s/U$ has a broader range of parameter values that satisfy experimental measurements compared to the $b = B_0$ model. These results indicate that experimental compatibility is difficult to achieve with the constant commitment rate model and is much easier to achieve with a tunable commitment rate.

2.7.1 Incompatible dynamics of $b = B_0$ model with experimental measurements for various Hill coefficients in nutrient feedback

To test the sensitivity of our results to the specific form of nutrient feedback, we altered the form of Equation 1 by choosing Hill coefficients in the division rate $a = a_m E_d^n/(1 + E_d^n)$ and the cell death rate $\Lambda = \Lambda_m/(1 + E_d^n)$ such that $n = 1$ or $n = 3$ instead of $n = 2$ (the current form of Equation 1).

We find that when the form of Equation 1 is altered to express Hill coefficients of values 1 and 3 instead of 2 (Figure S4), the $b = B_0$ model (Figure S4B,C) has no parameter values in the parameter space of (a_m, Λ_m) that satisfy all experimental measurements and linear stability criteria (see legend in Figure S4A). The black outlines in Figure S4 indicate values of (a_m, Λ_m) that satisfy experimental measurements of (1) division rate in homeostasis (blue), (2) maximum rate of symmetric-stem fate outcomes (red), and (3) time to reach approximate steady state according to conditions in Section 2.6 (white), see column 1 of Figure S4B-E. Note that for the $b = B_0$ model with $n = 3$, although there exists a small region outlined in Figure S4C, we see that linear stability analysis predicts that the solutions in this region do not reach homeostasis within physiological time (Figure S4C column 2) and that these solutions are highly oscillatory (Figure S4C column 3). When we examine solutions in this region of parameter space, the solutions are indeed highly oscillatory, and the identification of "homeostasis" by the conditions in Section s.6 is an artifact of the solutions which have oscillations of particular shapes.

We find that when the form of Equation 11 is altered to express Hill coefficients of values 1 and 3 instead of 2, a model with $b = B_0 s/U$ (Figure S4D and E) has a broad range parameter values (a_m, Λ_m) that satisfy all experimental measurements (column 1) as well as linear stability criteria (columns 2,3).

These results show that the $b = B_0$ model exhibits incompatibility of dynamics with experiments even when the precise form of feedback through E_d is altered in Equation 1. Additionally, the $b = B_0 s/U$ model exhibits improved compatibility with experiments compared to the $b = B_0$ model when the same alterations are

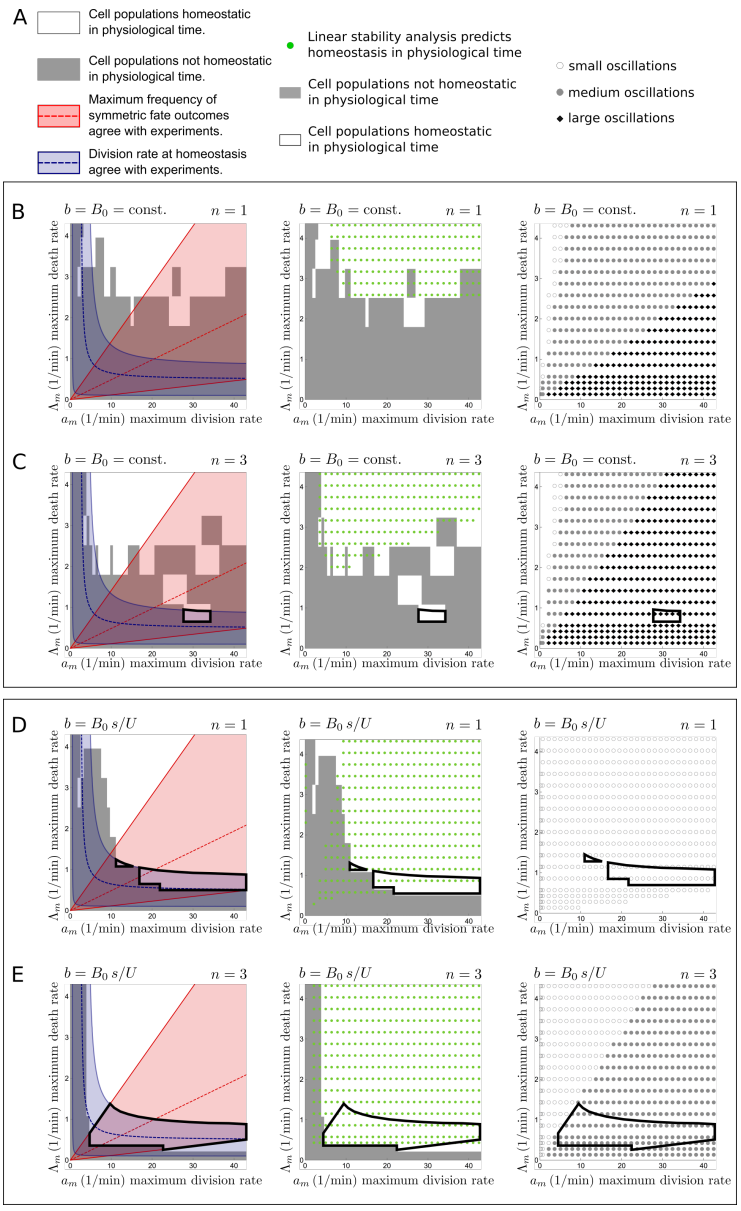

Figure S4: The $b = B_0$ model remains incompatible with experiment for various nutrient feedback Hill coefficients in Equation 1, while the $b = B_0 s/U$ model remains compatible with experiment for the same variations. (A) Legend for columns 1-3 of (B-E). (B-E) Parameter space (a_m, Λ_m) indicating compatibility or incompatibility with experiment for the $b = B_0$ model (B,C) and the $b = B_0 s/U$ model (D,E) with Hill coefficient $n = 1$ (B,D) and $n = 3$ (C,E) applied to the nutrient feedback for E_d in Equation 1.

made.

2.7.2 Incompatible dynamics of $b = B_0$ model with experimental measurements for various cellular consumptions A_1, A_2, and A_3

To test the sensitivity of our results to the specific values of nutrient consumption per cell in the three cell types, we altered the cellular consumption A_1, A_2, and A_3 belonging to stem cells, enteroblasts, and enterocytes in Equation 2 and solved Equation 1 for constant commitment rate ($b = B_0$) and commitment rate with feedback ($b = B_0 s/U$).

Since Equation 2 indicates that an overall factor of A_1 can be absorbed into E_{in}, we note that to vary the values of A_1, A_2, and A_3, we need only to vary the ratios A_2/A_1 and A_3/A_1. For this parameter exploration, we assume that $A_1 \leq A_2 \leq A_3$. This assumption is biologically practical, since stem cells are the smallest cells in the system, enteroblasts are larger than stem cells, and enterocytes are the largest. In Figures S5 and S6, we explored values of $(A_2/A_1, A_3/A_1)$ that vary over two orders of magnitude and that satisfy $A_2/A_1 \geq 1$ and $A_3/A_1 \geq 1$. We took values $(A_2/A_1, A_3/A_1) = (1,1)$, $(1,10)$, $(1,100)$, $(10,10)$, $(10,100)$, and $(100,100)$, and we solved Equation 1 for $b = B_0$ (Figure S5) and $b = B_0 s/U$ (Figure S6) for those values of A_2/A_1 and A_3/A_1. For Figure 2 of the main text and sections of the Supplement, we had chosen intermediate values of $(A_2/A_1, A_3/A_1) = (4,16)$, as the results of the model are not sensitive to this set of parameter values.

We show that for an extensive range of values of cellular consumption satisfying biological expectations ($A_1 \leq A_2 \leq A_3$), the model with $b = B_0$ exhibits very limited compatibility with experiment (Figure S5), while the model with $b = B_0 s/U$ (Figure S6) exhibits compatibility with experiment for a broad range of parameter space (a_m, Λ_m).

2.7.3 Solutions to model with commitment rate $b = B_0 s/(s+U)$ and $b = B_0 s/(s+u+U)$ are similar to solution to model with $b = B_0 s/U$

We can also examine altered forms of feedback to the commitment rate that depends on stem cell ratios of various forms. Here, we examine feedback of the form $b = B_0\, s/(u+U)$ and $b = B_0\, s/(s+u+U)$. The steady state solutions of these models are obtained by substituting $b = B_0\, s_0/(u_0+U_0)$ and $b = B_0\, s_0/(s_0+u_0+U_0)$ into Equations 4-6 and solving. Denoting $s_0/u_0 \equiv f_1$ and $s_0/U_0 \equiv f_2$, and noticing that $B_0\, s_0/(u_0+U_0) = (1/f_1 + 1/f_2)^{-1}$, we can

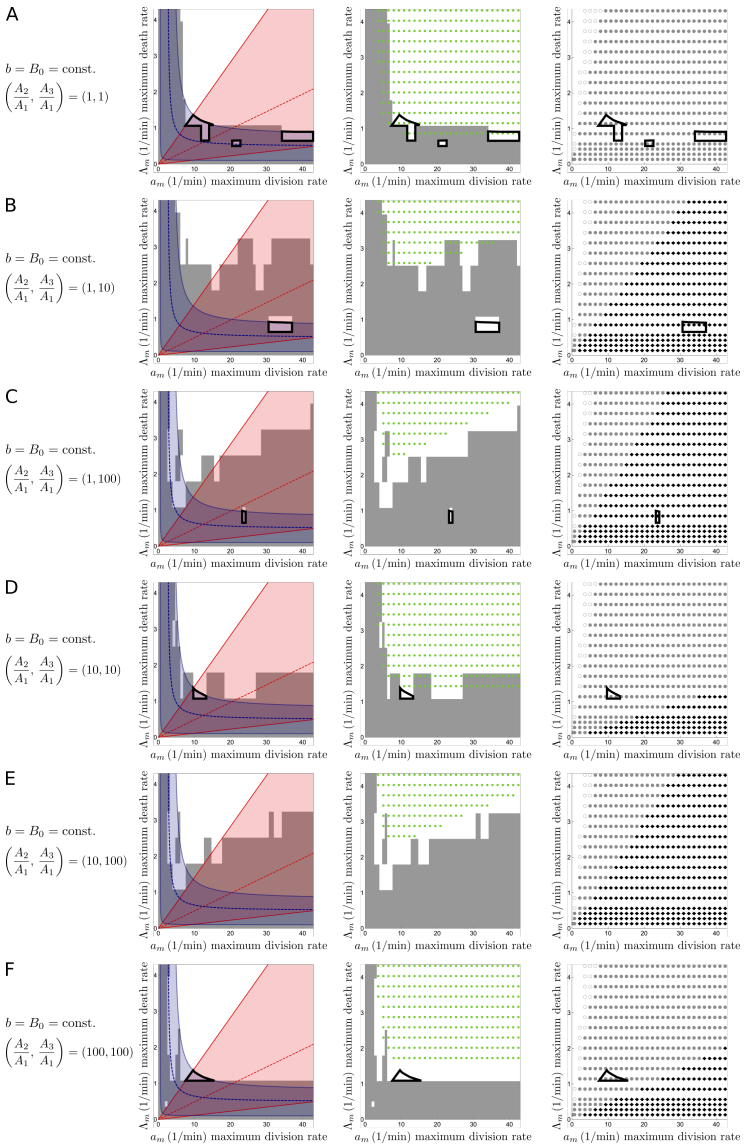

Figure S5: The constant commitment rate $b = B_0$ model has very limited parameter space that is compatible with experimental measurements (column 1) and linear stability criteria (columns 2,3) for various values of cellular consumption. Color coding as in Figure S4. (A-F) Parameter space (a_m, Λ_m) indicating compatibility or incompatibility with experiment for the $b = B_0$ model for $(A_2/A_1, A_3/A_1) = (1, 1)$ (A), $(A_2/A_1, A_3/A_1) = (1, 10)$ (B), $(A_2/A_1, A_3/A_1) = (1, 100)$ (C), $(A_2/A_1, A_3/A_1) = (10, 10)$ (D), $(A_2/A_1, A_3/A_1) = (10, 100)$ (E), and $(A_2/A_1, A_3/A_1) = (100, 100)$ (F).

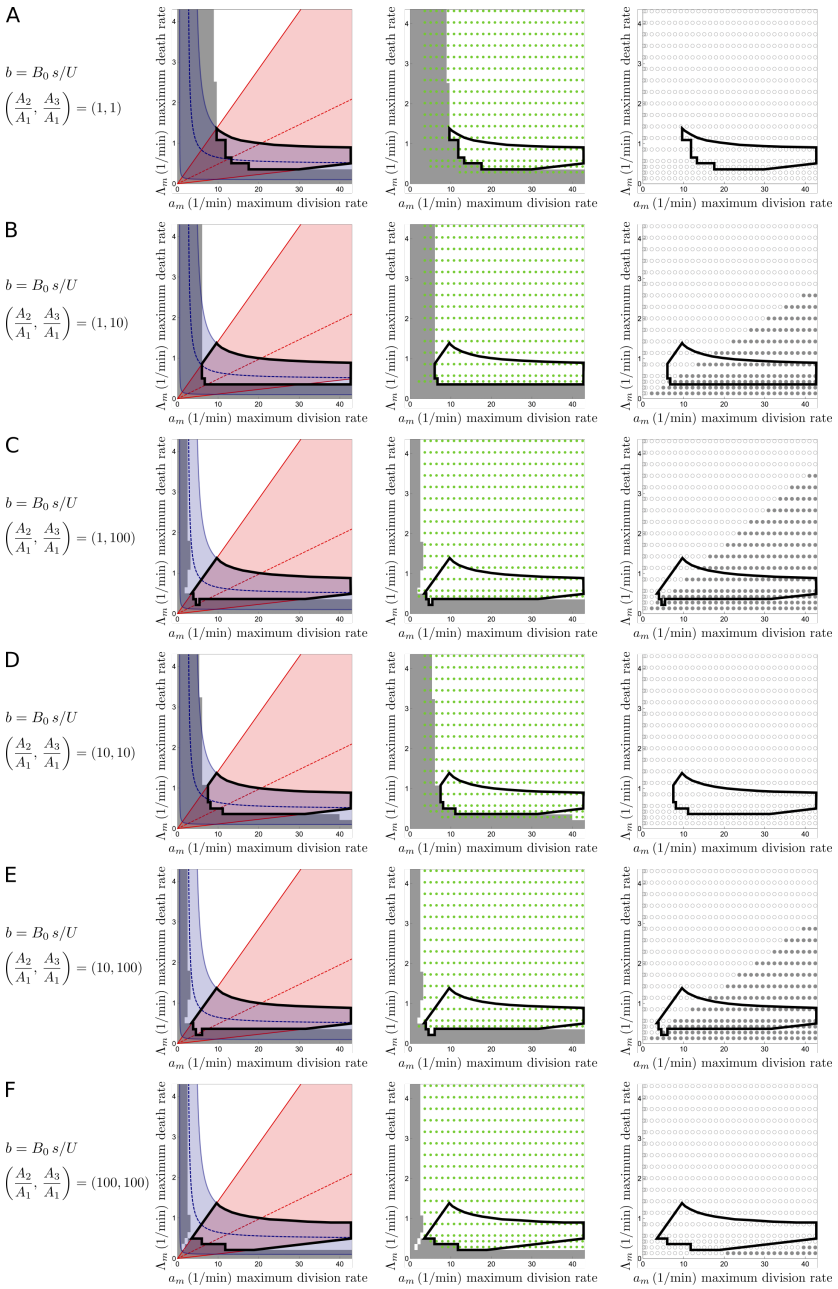

Figure S6: The feedback-dependent commitment rate $b = B_0 s/U$ model has broad parameter space that is compatible with experimental measurements (column 1) and linear stability criteria (columns 2,3) for various values of cellular consumption. Color coding as in Figure S4. (A-F) Parameter space (a_m, Λ_m) indicating compatibility or incompatibility with experiment for the $b = B_0 s/U$ model for $(A_2/A_1, A_3/A_1) = (1, 1)$ (A), $(A_2/A_1, A_3/A_1) = (1, 10)$ (B), $(A_2/A_1, A_3/A_1) = (1, 100)$ (C), $(A_2/A_1, A_3/A_1) = (10, 10)$ (D), $(A_2/A_1, A_3/A_1) = (10, 100)$ (E), and $(A_2/A_1, A_3/A_1) = (100, 100)$ (F).

rewrite Equations 4 and 5 for the case of feedback $b = B_0 s/(u+U)$ as:

$$f_1 = \frac{\lambda}{B_0}\left(\frac{1}{f_1}+\frac{1}{f_2}\right) \tag{23}$$

$$f_2 = \frac{\Lambda_m}{B_0}\left(\frac{1}{f_1}+\frac{1}{f_2}\right) - \frac{\Lambda_m}{a_m} \quad . \tag{24}$$

Rearranging Equations 23 and 24 to express f_2 as a function of f_1:

$$f_2 = \frac{\Lambda_m}{\lambda} f_1 - \frac{\Lambda_m}{a_m} \quad , \tag{25}$$

and noticing that Equations 23 and 24 can be rearranged to form a cubic equation for f_1:

$$f_1^3 - \frac{\lambda}{a_m} f_1^2 - \frac{\lambda}{B_0}\left(1+\frac{\lambda}{\Lambda_m}\right) f_1 + \frac{\lambda^2}{B_0 a_m} = 0 \quad , \tag{26}$$

solving for f_1, and choosing the positive, real root that gives rise to a value of $f_2 \leq 1$ (since we want a steady state solution with stem cells fewer than enterocytes), the steady state of the system is specified by the solution of Equation 26, together with Equation 25 and Equation 6 where b would be replaced by $b = B_0 \left(1/f_1 + 1/f_2\right)^{-1}$.

A similar analysis gives rise to the steady states for the feedback model $b = B_0\, s/(s{+}u{+}U)$ where we note that since $B_0\, s_0/(s_0{+}u_0{+}U_0) = (1 + 1/f_1 + 1/f_2)^{-1}$, the same analysis would proceed except with $(1/f_1 + 1/f_2)$ replaced by $(1 + 1/f_1 + 1/f_2)$ in Equations 23 and 24.

We can apply known experimental values of cell ratios in the biological system to Equations 23 and 24 by setting $f_1 = s_0/u_0 = 1$ and $f_2 = s_0/U_0 = 0.2$, similar to our analysis in the main text. This gives rise to exploration of parameter space (a_m, Λ_m) along with characterization of experimental compatibility related to (1) the number of divisions in homeostasis, (2) the maximum rate of symmetric-stem fate outcomes, and (3) time to reach homeostasis during resizing (Figure S7).

In Figure S7, we identify values of (a_m, Λ_m) that are compatible with experimenta for a model where the feedback to commitment rate has $b = B_0\, s/(u{+}U)$ (A) and a model where the feedback to commitment rate has $b = B_0\, s/(s{+}u{+}U)$ (B) (in similar style to Figure 2 in the main text). We show that with both forms of feedback in b, there remain large regions of parameter space that are compatible with experiment. Moreover, in these regions, solutions of the models (Figure S7C,D) are qualitatively similar to the solutions presented in Figure 2 of the main text where $b = B_0\, s/U$.

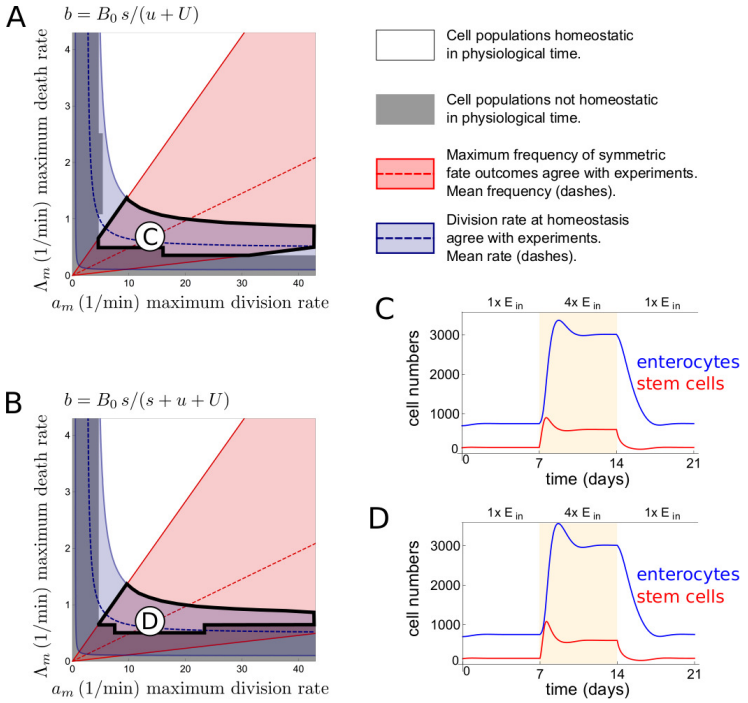

Figure S7: Models (Equation 1) with alternate feedback to commitment rate give similar results as $b = B_0\, s/U$ model; therefore, alternate feedback models remain compatible with experiment. (A-B) Regions of parameter space (a_m, Λ_m) that are compatible with experiment exist for both $b = B_0 s/(u+U)$ model (A) and $b = B_0 s/(s+u+U)$ model (B). (C-D) In the compatible region, solutions of alternate feedback models are non-oscillatory. Solutions to $b = B_0 s/(u+U)$ model (C) and $b = B_0 s/(s+u+U)$ model (D) indicating stem cell numbers (red) and enterocyte numbers (blue) as functions of time.

2.8 Model that combines u and U populations gives similar results as model with separate u and U populations in non-spatial analysis

A simplified version of the non-spatial model is presented here, in which the enteroblast (u) and enterocyte (U) populations are combined into a single population of cells, "differentiated cells", denoted by W. For this model system, we adapt the model equations as:

$$\begin{aligned} \dot{s} &= a_m \frac{E_d^2}{1+E_d^2} s - bs \\ \dot{W} &= bs - \Lambda_m \frac{1}{1+E_d^2} W \quad , \end{aligned} \tag{27}$$

where $E_d \equiv E_{\text{in}}/(A_1 s + A_4 W)$ is the nutrient density. Here, all differentiated cells experience cell death instead of only enterocytes. The steady state solutions s_0 and W_0 to the model with $\{s, W\}$ satisfy relationships analogous to Equations 5 and 6:

$$s_0/W_0 = \Lambda_m \left(\frac{1}{b} - \frac{1}{a_m} \right) \tag{28}$$

$$s_0 = \sqrt{\frac{a_m - b}{b}}\, E_{\text{in}} \Bigg/ \left(A_1 + A_4 \frac{1}{\Lambda_m} \frac{1}{\left(\frac{1}{b} - \frac{1}{a_m}\right)} \right) \quad . \tag{29}$$

In the case of $b = B_0$, we have that the full steady state of the system in Equation 27 is specified by Equations 28 and 29 above with b replaced by B_0. In the case where the commitment rate contains feedback with $b = B_0\, s/W$, we have that s_0/W_0 is given by the right hand side of Equation 16:

$$s_0/W_0 = \frac{-\Lambda_m}{2a_m} + \sqrt{\left(\frac{\Lambda_m}{2a_m}\right)^2 + \frac{\Lambda_m}{B_0}} \quad . \tag{30}$$

Equation 30 combined with Equation 29 in which b replaced by $B_0\, s_0/W_0$ gives the full steady state for Equation 27 with $b = B_0 s/W$.

We find that the simplified system in Equation 27 behaves similarly to the system in Equation 1. In particular, we find that if the $\{s, W\}$ model contains no feedback in the commitment rate ($b = B_0$), then the parameter space (a_m, Λ_m) has no region that is compatible with experiment and linear stability criteria (Figure S8A,A'). This is due to the highly oscillatory nature of solutions in the parameter space that satisfies experimental values of division rate and maximum frequency of symmetric-stem fate outcomes (Figure S8C). However, if feedback based on stem cell ratio is introduced into the commitment rate ($b = B_0\, s/W$), then solutions become less oscillatory (Figure S8D), and there exists parameter regions that satisfy all experimental measurements and linear stability criteria (Figure S8B,B').

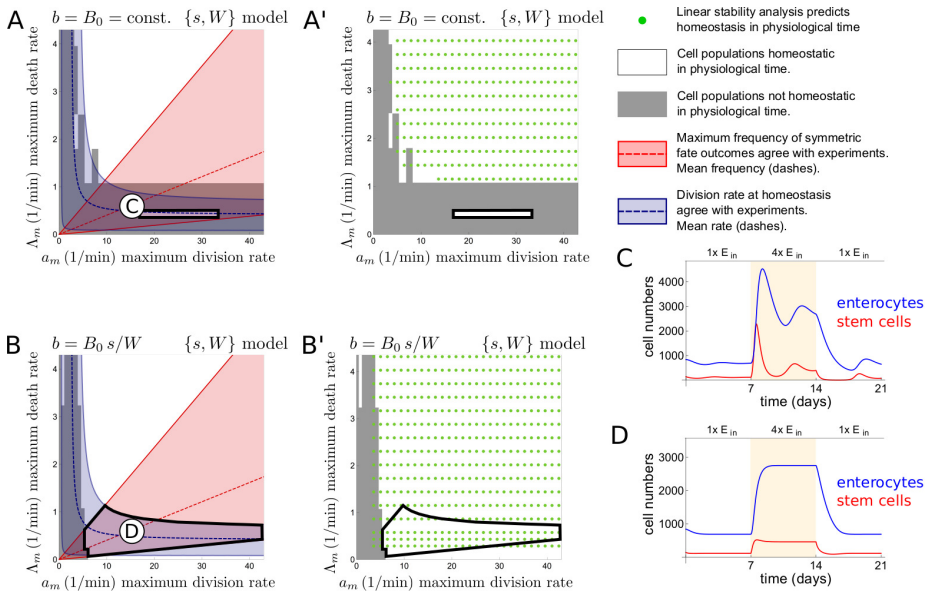

Figure S8: Non-spatial analysis of $\{s, W\}$ model (Equation 27) in which u and U cells are combined gives similar results as model with separate u and U cells. (A-B') Regions of parameter space (a_m, Λ_m) that are compatible with experiment do not exist for $b = B_0$ model (A,A') while they do exist for $b = B_0 s/(s+u+U)$ model (B,B') in the simplified $\{s, W\}$ system. (C) Solutions of $b = B_0$ model are highly oscillatory in parameter regimes that satisfy experimental values of division rate and maximum frequency of symmetric-stem fate outcomes. (D) Solutions of $b = B_0\, s/U$ model are not highly oscillatory in those parameter regimes.

2.9 Potential extension of model to include dependence of differentiation rate λ on $E_{\mathbf{in}}$

Our model in Equation 11 replicates the scaling of cell populations with total ingested nutrient in the midgut as well as other midgut dynamics. However, studies [2] have shown that in starved states, enteroblast numbers are suppressed compared to stem cell numbers and enterocyte numbers and therefore do not scale with them. Provided that the measurements of these cell numbers are made during homeostasis, to satisfy these measurements, we suggest an extended model in which enteroblast numbers do not scale in steady state. To obtain non-scaling of enteroblast numbers, we suggest that the model in Equation 11 be extended so that the differentiation rate λ depends explicitly on the total ingested nutrient E_{in} such that when E_{in} is large ("fed"), we have $\lambda = \lambda_0$, a constant value, but when E_{in} is small ("starved"), the value of λ increases sharply to a larger value. Assuming units in which "fed" guts receive $E_{\text{in}} \gtrapprox 4$ nutrients and "starved" guts receive $E_{\text{in}} \lessapprox 1$ nutrients, we suggest:

$$\lambda = \lambda_0 \left(1 + \frac{1}{1/2 + E_{\text{in}}^2}\right) \quad . \tag{31}$$

The specific form of Equation 31 does not sensitively influence the dynamics of the system. Substituting Equation 31 into Equation 11 gives the extended model. Note that this extended model preserves scaling in terms of the ratio of stem cells to enterocytes.

The interpretation of the extended model is the following: when the gut is sufficiently fed (E_{in} is sufficiently large), the rate of differentiation is constant ($\lambda = \lambda_0$). This is because enteroblasts are cells that are fully committed to a differentiation program; the rate of differentiation depends on the rate of execution of this program, and we assume that when nutrient is abundant, this rate is generally independent of nutrient. However, when nutrient is largely unavailable (E_{in} is small), the enteroblasts turn to a sped-up differentiation program $\lambda > \lambda_0$ to quickly increase the number of enterocytes in order to potentially increase ability to absorb nutrients. Importantly, in the extended model, the increase in differentiation rate associated with starvation would depend on total nutrient E_{in} and not on nutrient density. Biologically, this dependence would mean that when total nutrient is low, the gut senses this globally (perhaps through changes in mechanical pressure in the organ), and a change in differentiation rate for all enteroblasts is then adopted.

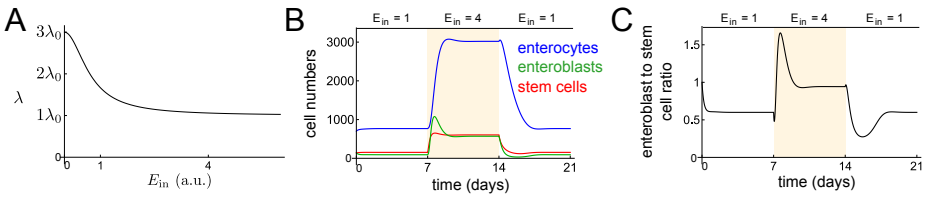

Figure S9: An extended model in which differentiation rate of enteroblasts depend on the input nutrients. (A) Differentiation rate λ as a function of E_{in} (Equation 31). (B,C) Cell population dynamics in the extended model using the same parameter values as Figure 2D in the main text: (B) cell numbers and (C) enteroblast-stem cell ratio as functions of time; the enteroblast-stem cell ratio is less than 1 during starved ($E_{\text{in}} = 1$) states.

3 Detailed description of 2-dimensional spatial model

3.1 Physical cell-cell forces

From the 2-dimensional model in the main text, we have:

$$\frac{d\mathbf{x}}{dt} = \eta \left(\sum_{n \in \text{n.n}} (\rho_n + \gamma_n) \hat{\mathbf{d}}_n + \sigma \mathbf{X}(t) \right) \quad . \tag{32}$$

where the sum on $n \in$ n.n indicates summing over nearest neighboring cells, quantities ρ_n and γ_n are magnitudes of repulsion and adhesion forces from neighbor cells, and $\mathbf{d}_n$ is a unit vector towards the neighbor cell. The self-generated random force $\mathbf{X}(t)$ has components sampled from a normal distribution $N(0, 1)$, and σ indicates the magnitude of the random force.

We take ρ to be simple linear repulsion that acts between cells only when they are touching. Let d denote the distance to the neighbor, and R_1, R_2 denote the radii of the two cells cells, then

$$\rho = \begin{cases} H \cdot (d - R_1 - R_2) & \text{if } d \leq R_1 + R_2 \\ 0 & \text{if } d > R_1 + R_2 \end{cases} \tag{33}$$

where H is the repulsion coefficient.

For adhesion γ, we assume that the adhesion energy of two adherent cells of radii R_1 and R_2 given a separation d between their centers is proportional to their "buried area", assuming spherical shapes in three dimensions for the cells, see Figure S10. We use the 3D buried area for adhesion energy when deriving the adhesion force to capture the fact that although cells move in 2D, we would

like to model them as spherical in morphology. The adhesion force is:

$$\gamma = \begin{cases} 0 & \text{if } d < \max(R_1, R_2) \\ \Gamma \cdot (R_1 + R_2)(d - R_1 + R_2)(d + R_1 - R_2)/d^2 & \text{if } \max(R_1, R_2) < d < R_1 + R_2 \\ 0 & \text{if } d > R_1 + R_2 \end{cases} \tag{34}$$

where Γ is the adhesion coefficient. We require that the adhesive force is non-zero only when the cells are touching, and we set the adhesive force to 0 when $d < \max(R_1, R_2)$ because we expect repulsive forces to be completely dominant at this distance. Note that γ simplifies to a constant $\gamma = 2\Gamma R$ if $R_1 = R_2 = R$.

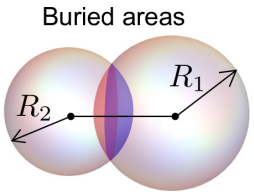

Figure S10: Schematic of "buried area". The adhesive energy between two cells with radii R_1 and R_2 is modeled as proportional to their "buried area" in three dimensions, which are the areas of the spherical caps that exist in the overlap of the two cells.

3.1.1 Non-dimensionalization of protein z equation

A fully-dimensional form of the dynamics for protein z is:

$$\frac{dz}{dt} = p\left(\frac{z^m}{K^m + z^n(t)}\right)\left(\frac{K_2^k}{K_2^k + (\sum_n z_n(t - t_n))^k}\right) - \beta z \quad . \tag{35}$$

In the 2D model, we use units of minutes for t for convenient comparison between the non-spatial model and the 2D model (often converted to units of days in the main text). We use K as unit of concentration in which to express z so that $z = z'K$ such that z' is a unitless number. Then we rewrite Equation 35 as:

$$K\frac{dz'}{dt} = p\left(\frac{K^m z'^m}{K^m + K^m z'^m(t)}\right)\left(\frac{K_2^k}{K_2^k + (\sum_n K z'_n(t - t_n))^n}\right) - \beta K z' \quad . \tag{36}$$

Multiplying the above by $1/K$, and simplifying, we have:

$$\frac{dz'}{dt} = p\frac{1}{K}\left(\frac{z'^m}{1 + z'^m(t)}\right)\left(\frac{1}{1 + (\sum_n K/K_2 z'_n(t - t_n))^k}\right) - \beta z' \quad . \tag{37}$$

Denoting $p' = p/K$ and $g_n = K_2/K$, we have for dimensionless z' and p':

$$\frac{dz'}{dt} = p' \left(\frac{z'^n}{1 + z'^n(t)} \right) \left(\frac{1}{1 + (\sum_n z'_n(t - t_n)/g_n)^k} \right) - \beta z' \quad . \tag{38}$$

Removing primes from our notation, we obtain the equation for dimensionless protein concentration z (with time in minutes) in Equation 11 of the main text.

3.2 Tables of parameter values for non-spatial model and 2D simulations

First, we list our dimensional units and their typical measured values in Table 1. Then, we present numerical parameter values that are expressed in those units in Table 2.

Table 1: Dimensional units

unit	dimensions	description	typical empirical value
ℓ_0	length	enterocyte diameter	10μ
η	length/(time$\cdot$ force)	cell mobility	unknown for this tissue
K	$1/\text{length}^3$	switch-point concentration of fictitious protein z	unknown

Table 2: Numerical value of parameters used in non-spatial model and in 2D simulations

parameter	description	numerical value
a_m	max. division rate	0.0087 /min
Λ_m	max. death rate	0.00063 /min
λ	maturation rate	0.0025 /min
ρ	magnitude of repulsive force	$14\ell_0/\text{min}\eta$
γ	magnitude of adhesive force	$1\text{–}2.5\ell_0/\text{min}\eta$
σ	magnitude of motile force	$0\text{–}0.3\ell_0/\text{min}\eta$
p	Delta-Notch (DN) production	$7K$ /min
g_n	neighbor DN signaling switch point	$1K$
t_n	time delay for DN signaling	2 min
β	decay rate of z protein	1 /min

3.3 Implementation of division, cell death, and cell growth in the 2D spatial simulations

In 2D simulations, to physically and smoothly interpolate between stem cell, enteroblast, enterocytes, and $\varnothing$ states of cells, we assume that enteroblasts increase their size smoothly from stem cell-size R_s to enterocyte-size ℓ_0, and that apoptosing cells leave the model epithelium by shrinking smoothly in size over the course of realistic time scales. That is, denoting cell radii by as functions of time $R(t)$, we have:

$$\dot{R}_u = G_b \text{ with } R_s < R_u < \ell_0 \quad \text{enterobloasts} \tag{39}$$

$$\dot{R}_{\text{apoptosis}} = -A_{\text{pop}} \quad \text{apoptosing cells} \quad . \tag{40}$$

For stem cells and enterocytes that are not apoptosing, we have:

$$R_U = \ell_0 \quad \text{enterocytes} \tag{41}$$

$$R_s = 0.25\ell_0 \quad \text{stem cells} \quad . \tag{42}$$

The implementation of the 2D simulation fixes the rates G_b and A_{pop} at physiological values $G_b = 0.0025\,/\text{min} = (1/7)\,/\text{hour}$ and $A_{\text{pop}} = 0.017\,/\text{min} = 1\,/\text{hour}$.

For the consumption constants A_1, A_2, and A_3, we take these values to be proportional to cross-sectional areas of stem cells, enteroblasts, and enterocytes, i.e.

$$A_1 = R_s^2 = 0.25^2\ell_0^2 \quad , \quad A_2 = R_u(t)^2 \quad , \quad A_3 = \ell_0^2 \tag{43}$$

as rough estimations of consumption of food input E_{in}. The non-dimensionalizing factor E_d^0 to form $E_d = E_d^{\text{dim}}/E_d^0$ used in the simulations was 100.0 so that numerical inputs for the value of E_{in} were conveniently $\mathcal{O}(1)$.

3.4 Implementation of Delta-Notch equation in 2D simulations

Our Delta-Notch equations are delay equations and therefore need specification of initial time course $z(-t_n < t \leq 0)$ as initial conditions, where t_n is the delay time for signaling from a neighbor cell. When a cell divides at time T, the historical values of the protein z for times $T - t_n < t \leq T$ are copied to the daughter cells. Noise asymmetry is introduced when copying the historical values of z to the two daughters to mimic biological asymmetries in protein segregation during cell division. The amount of noise introduced in this initial condition for z for the two daughter cells, along with other parameters in the Delta-Notch equations and dynamics of physical contact, determines the average time a commitment decision is made through time evolution of z.

3.5 Details related to analysis of stem cell territory T

3.5.1 Correspondence between amplitude of motile noise and territory size

In simulations of the two-dimensional model, different values of the intrinsic stochastic motile force parameter for stem cells and enteroblasts ($\sigma_{\mathrm{sc,eb}}$) and for enterocytes (σ_{EC}) results in different computed values of stem cell territory T. Table 3 indicates the values of T and its natural logarithm ($\ln(T)$) used in Figure 5B of the main text that arise from different combinations of $\sigma_{\mathrm{sc,eb}}$ and σ_{EC}. Table 3 specifies simulations where adhesion values are $\gamma_{\mathrm{sc,eb}} = \gamma_{\mathrm{EC}} = 1\ell_0/\mathrm{min}\eta$ between cells. Based on replicate simulations with the same set of parameter values, the spread in T for given values of $\sigma_{\mathrm{sc,eb}}$, σ_{EC}, $\gamma_{\mathrm{sc,eb}}$, and γ_{EC} is approximately 0.1 (unitless).

Table 3: Correspondence between amplitude of motile noise σ and territory values

$\gamma_{\mathrm{sc,eb}} = \gamma_{\mathrm{EC}} = 1\ell_0/\mathrm{min}\eta$

$\sigma_{\mathrm{sc,eb}}$	0		0.05		0.1		0.2		0.3	
σ_{EC}	$\ln(T)$	T	$\ln(T)$	T	$\ln(T)$	T	$\ln(T)$	T	$\ln(T)$	T
0	-0.34	0.71	-0.18	0.83	-0.026	1.0	0.28	1.3	0.54	1.7
0.05	0.15	1.2	0.25	1.3	0.29	1.3	0.47	1.6	0.73	2.1
0.1	0.37	1.4	0.55	1.7	0.58	1.8	0.75	2.1	0.86	2.4
0.2	0.89	2.4	0.91	2.5	1.0	2.8	1.2	3.3	1.6	4.9
0.3	2.1	8.5	2.3	10.	2.4	11.	2.7	15.	3.1	21.

3.5.2 Stem cell scaling emerges for sufficiently large values of stem cell territory

To determine whether a particular set of parameters for motility σ and adhesion γ specify a system that exhibits stem cell scaling, we ran two simulations for each set of values σ and γ: one in which the input nutrients is $1 \times E_{\mathrm{in}}$ and one in which the input nutrients is $2 \times E_{\mathrm{in}}$. If the system exhibits stem cell scaling, then the ratio of stem cells to enterocytes for the $1 \times E_{\mathrm{in}}$ simulation (F_1) should be equal to the ratio of stem cells to enterocytes for the $2 \times E_{\mathrm{in}}$ simulation (F_2). That is, for perfect scaling, we have $F_1 = F_2$. We compute the fractional difference F between the resultant stem cell ratios for the two simulations as

$$F = \frac{|F_1 - F_2|}{\frac{1}{2}(F_1 + F_2)} \quad . \tag{44}$$

Values of F indicated as a function of $\ln(T)$ are indicated in Figure S11 for various values of adhesions γ. Stem cell scaling occurs when differences F are close to 0.

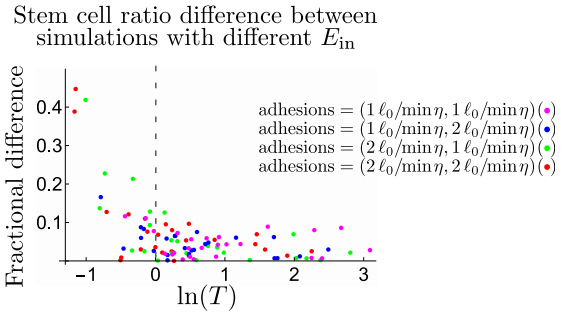

Figure S11: Stem scaling holds for stem cell territory T larger than a threshold value (dotted line). Plot indicates difference, computed as a fraction (y-axis), between stem cell ratios for simulations with different input values of E_{in}, as a function of $\ln(T)$ (x-axis).

3.5.3 Stronger correspondence between 2D simulations and non-spatial model for larger values of stem cell territory

To compute a fit of the non-spatial $b = B_0 s/U$ model to the 2D simulation, we computed the value of B_0 from Equation 13, substituting the simulated value of the stem cell-enterocyte ratio for the expression s_0/U_0. We obtain the model time course for $s(t)$, $u(t)$, and $U(t)$ by then solving Equation 11. Denoting the simulation time courses for cell numbers as $s_{\text{sim}}(t)$, $u_{\text{sim}}(t)$, and $U_{\text{sim}}(t)$ for stem cells, enteroblasts, and enterocytes, we compute the discrepancy between simulation and model cumulatively as:

$$\Delta_N = \frac{1}{3}\left(\frac{\int dt\,|s(t) - s_{\text{sim}}(t)|}{\int dt\, s(t)} + \frac{\int dt\,|u(t) - u_{\text{sim}}(t)|}{\int dt\, u(t)} + \frac{\int dt\,|U(t) - U_{\text{sim}}(t)|}{\int dt\, U(t)}\right) \quad . \tag{45}$$

Similarly, denoting $b_{\text{sim}}(t)$ as the rate of commitment that emerges from the 2D simulation, and using $b(t) = B_0 s(t)/U(t)$ as the commitment rate specified in the non-spatial model, we have the cumulative discrepancy in commitment rate between simulation and model:

$$\Delta_b = \frac{\int dt\,|b(t) - b_{\text{sim}}(t)|}{\int dt\, b(t)} \quad . \tag{46}$$

The disprepencies between simulation and model Δ_N and Δ_b as functions of $\ln(T)$ are indicated in Figure S12 for various values of adhesion parameters. Figure 5C-D of the main text shows Δ_N and Δ_b as functions of $\ln(T)$ only for the adhesion parameters $\gamma_{\text{sc,eb}} = \gamma_{\text{EC}} = 1\ell_0/\min\eta$.

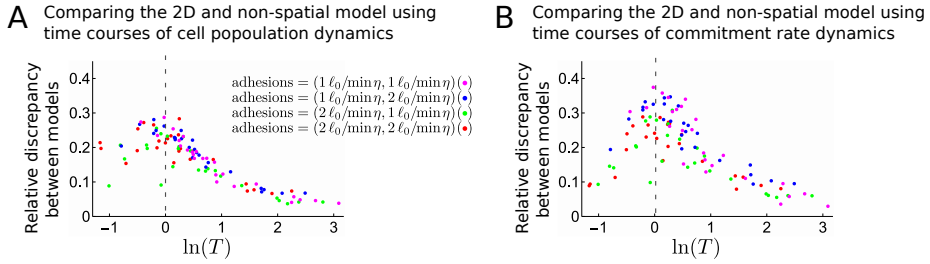

Figure S12: Stronger correspondence between 2D simulations and non-spatial $b = B_0 s/U$ model for large T. (A) Plot indicates relative discrepancy, computed as a score between 0 and 1 (y-axis), in time courses of cell number dynamics, between a 2D simulation and the $b = B_0 s/U$ model fitted to it for various values of adhesion. (B) Plot indicates relative discrepancy, computed as a score between 0 and 1 (y-axis), in time course of commitment rate b dynamics, between a 2D simulation and the $b = B_0 s/U$ model fitted to it for various values of adhesion.

3.5.4 Analysis of simulated cell tracks

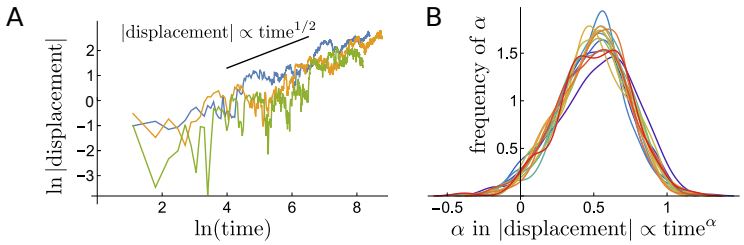

Figure S13: Stem cells in 2D simulations generally execute diffusive motion. (A) Logarithm of magnitude of displacement as a function of logarithm of time for three sample simulated stem cell tracks showing that tracks mostly follow a diffusive model $|\text{displacement}| \propto \text{time}^{1/2}$ (black line). (B) Histogram of exponents α of tracks fitted to model $|\text{displacement}| \propto \text{time}^{\alpha}$; different lines correspond to stem cells that terminally committed during different time intervals of same simulation. Mean of α distribution is $\text{Mean}(\alpha) = 0.50$, compatible with diffusion model.

To obtain the diffusion coefficient (Equation 13 of the main text) for stem cell tracks from simulations, we plot the magnitude of displacement of the stem cells (based on their position) as a function time in a log-log plot. We fit to the stem cell tracks the model $|\text{displacement}|^2 \propto D \cdot \text{time}$. We extract the coefficient D as the diffusion constant. To obtain the distribution of α in Figure S13B, we fit the stem cell tracks to the model $\ln|\text{displacement}| = \alpha \ln(\text{time}) + \text{const.}$. Plotting several sample simulated tracks (Figure S13A) and examining the distribution of α values for the ensemble of stem cell tracks Figure S13B), we find that stem

cells on average follow a diffusive model, i.e., Mean(α) = 0.50. However, they execute a broad range of behaviors in the simulations, as the width of the α distribution is large, i.e., $\sqrt{\text{Var}(\alpha)} = 0.24$.

References

[1] N. Buchon, D. Osman, F. P. David, H. Y. Fang, J.-P. Boquete, B. Deplancke, and B. Lemaitre, "Morphological and molecular characterization of adult midgut compartmentalization in Drosophila," *Cell reports* **3** (2013), no. 5 1725–1738.

[2] L. E. O'Brien, S. S. Soliman, X. Li, and D. Bilder, "Altered modes of stem cell division drive adaptive intestinal growth," *Cell* **147** (2011) 603–614.